EQC Postdoctoral Fellowship Final Report

Aaron Wech

March 8, 2013

Acknowledgments:

This postdoctoral research was supported by funding from the EQC. Additional thanks to my various coauthors of submitted/published papers, to Donna Eberhart-Phillips for providing tomography code, and to Victoria University and GNS Science for hosting and facilitating my research efforts.

Casual Abstract:

My EQC postdoctoral research was divided into two projects that focused on different seismic hazards in New Zealand: the southern Hikurangi subduction zone and the Alpine Fault. For the subduction zone, we used the signals from earthquakes and explosions to image the plate boundary at depth and investigate how plate geometry, materials, and background seismicity relate to crustal faulting, plate coupling and megathrust earthquake hazard. Secondly, we investigated the central section of the Alpine Fault, which is inferred to be locked, quiet and late in its earthquake cycle. With our discovery of tremor, a low-pitched seismic reverberation emanating from the fault, we present the 1st evidence of any present-day deformation along the transform plate boundary with implications for earthquakes in the locked zone above.

PART I – Hikurangi Subduction Zone

Technical Abstract:

The passive and active-source Seismic Array HiKurangi Experiment (SAHKE) investigated the structure of the forearc and subduction plate boundary beneath southern North Island along a 350 km transect. We used 92 onshore seismographs and 20 ocean-bottom seismographs to record >69,000 shots of a 400 km marine multichannel seismic-reflection survey, and then recorded 12 borehole explosive sources (350-500 kg) distributed approximately 8 km apart on 835 onshore seismographs. Tomographic inversion of first arrival travel times was used to derive a P-wave image of the crust that is resolved to 20-25 km depth, which was combined with refracted phases and migrated reflection events to image subducting slab geometry and crustal structure. Offshore, the subducted Pacific Plate oceanic crust is recognized from its high positive velocity gradient, but it becomes less distinct beneath the onshore Tararua Ranges, where the interface increases in dip at about 15 km depth from <5° to >15° farther west. This bend in the subducted plate is associated with vertical clusters in seismicity, splay fault branching above, and low-velocity high-attenuation material that we interpret to be underplated subduction channel material. We infer a step down in the decollément that transfers slip on the plate interface to the top of subducted oceanic crust. We suggest that this drives local uplift of the Tararua Range, and corresponds to an important lateral change in hydrological conditions at the plate interface. The change in dip of the Hikurangi subduction interface at 10–20 km depth is also spatially correlated with the transition from geodetically determined locked to unlocked areas of the plate interface and partitions stable and unstable slip regimes.

1. Foreword

This report reiterates the findings presented in *Henrys et al.* [2013], of which I am the second author. I'll attempt to summarize some of the key points—with an emphasis my contributions through body wave tomography—but most of details and discussion reside in that comprehensive manuscript. Much of the text below, in fact, is blatantly copied from that manuscript, as I didn't see much value in rewording text that was carefully crafted for the peer review publication process. My contributions are mostly in creating the velocity model, which I don't view as a ground-breaking result by itself, but it is the highest resolution velocity image we have in this region and is invaluable for interpretation when combined with the host of other geophysical observations in this data set.

2. Introduction

Subduction zones produce the largest earthquakes and tsunamis on Earth, as evidenced by the 2011 Tohoku Mw 9.0 earthquake [*Simons et al.*, 2011] and 2004 Sumatra Mw 9.3 earthquake [*Ammon et al.*, 2005; *Lay et al.*, 2005]. The fault slip behaviour on subduction thrust faults varies greatly between subduction zones, and along-strike at the same subduction zone. Our study aimed to image and resolve the physical properties of a locked subduction thrust that may fail in a future large earthquake in the Wellington region of New Zealand [*Wallace et al.*, 2009], so that we may better understand the mechanics of slip on a subduction thrust.

To investigate the physical parameters controlling locking on the Hikurangi plate interface and to determine geometrical relationships with secondary faults, we undertook a controlled-source and passive (earthquake) seismic imaging experiment in the Wellington region. The Seismic Array HiKurangi Experiment (SAHKE) imaged the plate interface beneath southern North Island with onshore-offshore marine active-source seismic data from 3 sides, onshore shots, and local and teleseismic earthquakes (Figure 1). We present a preliminary analysis of this large dataset. Onshore-offshore wide-angle seismic- reflection and refraction data are analysed to constrain the first detailed 2-dimensional tomographic model of P-wave structure across a transect of the southern Hikurangi margin orthogonal to the Australia/Pacific plate boundary. This model places constraints on key parameters such as Moho geometry, subducting slab geometry and forearc structure, which may modulate the location of plate coupling. The available raypaths provide strong constraints on the absolute velocity of the shallow plate boundary to 25 km depth. The

SAHKE transect data provide additional insight into plate interface coupling and upper crustal splay faults that are fundamental to our understanding of subduction zone architecture.

3. Method: First arrival tomography

We picked first arrivals from SAHKE01 and SAHKE02 shots into all OBS and transect surface seismometers. These arrival data were combined with first arrivals from 12 SAHKE II land explosion shot gathers, totalling 17,773 travel times. We model this collection of first-arrival travel times from all available transect data by inverting for P-velocity structure using existing tomographic methods [*Eberhart-Phillips*, 1990; 1993; *Thurber and Eberhart-Phillips*, 1999]. The tomographic method solves along ray paths in three-dimensions, but we choose a large out-of-transect-plane grid-node spacing to effectively create a 2-dimensional parameterization of velocity structure. Z-nodes sample the near surface at 1 km intervals from +1 km to -1 km throughout the inversion scheme. Elsewhere, we employ a progressive node spacing refinement scheme starting from 15 and 5 km intervals down to 2 and 1.5 km spacing in the transect and vertical directions, respectively.

We start with a 1-dimensional regional velocity model (Figure 2). Offshore, this starting model is modified to account for bathymetry and sediment velocities. From the seabed to a depth of 12 km, we set our initial velocity model to a spatial average of velocities determined by optimal migration and stacking of MCS data [*Henrys et al.*, 2013].

Between each of the 6 grid refinements, we perform 3 progressive inversions, allowing each node to vary by a maximum of 0.3 km/s. As the inversion steps progress, nodes that exceed velocities > 8 km/s are forced to 8 km/s and held fixed for subsequent inversions. The root mean square (RMS) travel time residual was reduced from 0.45 s to 0.04 s after 18 iterations (Figure 3). A 2-dimentional grid of derivative weight sum (DWS), which is a relative measure of the ray distribution [*Toomey and Foulger*, 1989], was constructed and used to discriminate between constrained and unconstrained regions of the first-arrival model (Figure 4). The DWS weights each ray path length according to its spatial separation from the grid node. Larger DWS values indicate better data coverage.

4. First-Arrival Resolution Test

A series of checkerboard tests were used to estimate the spatial resolution of the first-arrival

tomography results. Using the source-receiver geometry of the data along the SAHKE transect, synthetic data were generated for a series of known models to test the recovery of velocity perturbations by the inversion at various resolutions. These models consist of alternating anomaly patterns of ± 0.3 km/s perturbations superimposed on the starting model used for first-arrival tomography. The anomaly pattern function has the form sin(x)sin(z). We test both shallow and deep resolution by imposing fine and coarse checkerboard grid perturbations, respectively (Figure 5). The synthetic data were then inverted in the same manner as the real data. In order to quantify how much of the ± 0.3 km/s velocity perturbations were recovered, the starting model was subtracted from the final models.

The 15 x 10 km (horizontal and depth) checkerboard analysis (Figure 5b) shows that shallow structure is well resolved in the upper crust down to about 20-25 km depth beneath the SAHKE II land explosions and SAHKE01 offshore shots. At greater depths, fewer rays (Figure 4a) result in poorer resolution, but broad scale (35 x 20 km) structure is recovered. However, while the overall perturbation pattern is preserved, the inversion has difficulty in recovering positive velocity anomalies at depth.

5. Results

Offshore-onshore receiver gathers and were analyzed by Stuart Henrys and combined with my velocity model to interpret plate geometry and crustal structure [*Henrys et al.*, 2013]. Many stations have clear arrivals at offsets >150 km. East and west coast receiver gathers for the central station TS030, coincident with shot point 9, are shown in Fig 6 as one "supergather" [*Okaya et al.*, 2002]. Wide-angle phases are received from both airgun profiles SAHKE01 and SAHKE02 and can be viewed as a split-spread shot gather, that is, as if the source was at TS030 and receivers at each shot point. Including shot point 9 from the second phase of SAHKE (collocated close to station TS030) completes the supergather.

Onshore and from the eastern (trench) side, diving waves associated with sedimentary basins (Pg) are prominent on near offsets (transect distance 200 km). In the west, diving waves in the Australian continental crust (Pg) are visible to offsets of 100 km (transect distance 100 km). Prominent pre-critical wide-angle reflections (PintP) are observed a few seconds after Pg from the plate interface and are identified as the brightest and deepest of the band of crustal reflectivity observed at 8 s vertical offset on shot 9 (Figure 6b). PintP together with other crustal

phases merge to the west and cross over with PmP at transect distance 100 km. On the east coast we are able to differentiate the plate interface from the top of the oceanic Hikurangi Plateau (PtopP), which doesn't appear on near offsets but is more prominent on stations located east of Featherston and at offsets >50 km. Offshore MCS data (SAHKE01; Figure 6e) across the Hikurangi Trough image the active plate décollement (PintP) at ~10 km deep or 5-6 s two-way-travel-time (twt). Beneath the décollement, up to 2 s twt of Mesozic sequences (MES) are being subducted along with underlying oceanic rocks of the Hikurangi Plateau.

Phases interpreted as reflections from the base of the downgoing Hikurangi oceanic crust (PbaseP) are identified on OBS data from the Hikurangi Trough and on land receivers from shots west of Featherston and across the Tararua Range, but are less clear on onshore-offshore gathers across the west coast (Figure 6). PmP arrivals associated with Australia crust Moho are prominent on west coast onshore-offshore gathers at offsets >100 km, but the crossover of PintP and PmP at transect distance X=110-120 km results in a region of complexity in coda on the receiver gathers. Also at X=60-70 km diffracted arrivals (PdP) appear to originate from the Moho reflection. Reflections at c. 10 s twt are visible on MCS data from the western offshore sector of the transect, and these are consistent with being Australian Plate crust Moho (SAHKE02, Figure 6e). Onshore- offshore data from SAHKE02 also record Pn arrivals at offset >150 km (X=25-40 km in Figure 6) with apparent velocity of 8.0 km/s in the mantle of the Australian Plate. In the east OBS (not shown) record large-offset (> 200 km) Pn phases with very high (>8.5 km/s) apparent velocity interpreted as refracted phases through the mantle (and/or lower crust) beneath the Hikurangi Plateau. Especially prominent on onshore data are pre-critical lower crustal (PcP) reflections observed at 7-8 s twt beneath shot-points 9 to 12 and between distances 140 and 240 km along the transect (Figure 6).

6. Previously published velocity model comparison

Our first-arrival velocity model along the SAHKE transect is similar to but also differs in several respects from the 3-dimensional earthquake tomography model previously published [*Eberhart-Phillips and Reyners*, 2012]. Figure 7 shows the two velocity structures. The active source first-arrival velocity structure has resolved more detail in the shallow crust and images higher velocities in the Australian Plate. In general, we do not observe the broad lateral velocity variations that mark terrane boundaries as proposed by *Eberhart-Phillips and Reyners*, [2012],

but instead we attribute fine-scale lateral variations to faulted structures. The significant difference is the low velocities (< 6.5 to 7.0 km/s) in the lower crust and in the crust of the subducting Pacific Plate observed in our model to 40 km depth. The central region of the transect is not well resolved below 25 km but low Vp in the subducting crust was not observed in earthquake tomography. This study and the *Eberhart-Phillips and Reyners,* [2012] study use the same tomography code, but different input data. It is outside the scope of this paper to do a 3D inversion of all active-source (reflected and refracted phases) and earthquake data combined from the region.

7. Interpretation

Marine seismic line SAHKE01 images the trench slope and active plate décollement (PintP) at ~10 km deep [*Henrys et al*., 2013] coinciding with the upper part of a condensed sequence of strongly reflective Late Cretaceous-Early Oligocene (70-32 Ma) nannofossil chalks and alternating mudstones – referred to in previous work as sequence Y [*Davy et al.*, 2008]. Beneath the décollement, up to 3.5 km of Mesozic sequences are being subducted along the Hikurangi margin (MES of Davy *et al.* [2008]) together with underlying oceanic rocks of the Hikurangi Plateau. Pre-stack depth migration (PSDM) of PEG019, south of SAHKE01 (Figure 1), shows that the Cretaceous and Paleogene sedimentary rocks constitute a ~3.5 km thick subduction channel beneath the active plate boundary thrust dipping ~2° landward and roofed by the Y reflector [*Plaza-Faverola et al.*, 2012].

The lower crust beneath the Taraura Range is imaged as a low-velocity triangular zone with multiple reflectors, and is interpreted as an imbricated sequence of layers 10 km thick above the subduction interface at ~25 km depth. *Henrys et al.* [2013] stacked reflection section suggests this zone contains multiple west-dipping layers up to ~2 km thick with reflective boundaries. Such stacked slices should be anisotropic, with an axis of symmetry that is perpendicular to the plate boundary, which was suggested by *Savage et al.* [2007] from 24-28 km depth in the model TAR, based on forward modeling of receiver functions. A ramp structure in the deepest slice coincides with a 10° increase in dip of the subducted plate, which we interpret as a step down in the active subducting plate decollément at transect distance X=180 km, where west-dipping splay faults are inferred [*Henrys et al*., 2013]. Another pronounced splay fault (A) cuts the top of the imbricate sequence at 15-20 km depth and projects to the surface as the Wairarapa fault.

We propose a continuation beneath North Island of the subduction channel imaged at the eastern end of the transect. The step down of the active plate interface at X=180 km, inferred from reflector geometry, may represent a transfer of slip to the top of the oceanic crust and would allow low-velocity and low-density Cretaceous and Paleogene strata to be underplated. We propose that continued plate convergence has stacked imbricated sheets and driven uplift of the Tararua Range.

The step down is also spatially correlated with the geodetically inferred transition from locked to stable sliding. The relationship between this underplating and slow slip, however, remains unclear. For example, at Nankai high Poisons ratio >0.30 (Vp/Vs >1.9) in the subducted oceanic crust is indicative of high pore fluid pressure likely to generate slow slip [*Kodaira et al.*, 2004]. At southern Hikurangi Vp/Vs >1.8 are in the subducting crust below the locked part of the interface. Also at Cascadia slow slip and tremor may be facilitated by trapped fluids and high pore fluid pressures in underplated subducted sedimentary rocks [*Calvert et al.*, 2011], yet southern Hikurang slow slip is observed west of underplating observed on the SAHKE transect. However, we cannot rule out the deeper sections of the imaged Wairarapa fault as a source of slow slip observations beneath Kapiti Island. Furthermore, underplating is observed further north along the margin offshore Hawke Bay [*Henrys et al.*, 2006] and Raukumara [*Bassett et al.*, 2010] in unlocked regions of the margin. This would suggests that underplating of sediments is not a strong discriminate of geodectic behaviour on the plate interface and calls into question the relationship of high Vp/Vs to the occurrence of slow slip.

However, changes in subduction dip may provide a first order structural change along the strike of the Hikurangi subduction that best explains the locking pattern where increase in dip to angles greater than 8° defines a transition from locked areas of the plate interface to unlocked and partitions stable and unstable slip regimes. Along the margin we have found this change in dip also corresponds to a steepening of the topographic slope to greater than 3° seaward of the kink [*Barker et al.*, 2010] and is a locus of inherent weakness in the subducting slab where the occurrence may relate to a northward increase in subduction rate that controls initial slab dehydration and fluid release. If the locked zone slips, either as an earthquake or aseismic event, but if the updip segment, seaward of the plate bend, does not slip, then compressive stresses in the upper plate will be localized at this point. Indeed, this is where we observe thrust faults

ramping up from where the dip of the plate boundary interface increases and faults step down allowing underplating of sedimentary channel material to stack up. Permanent inelastic strain is manifested in the Wellington region as faulting and folding in the overriding plate for the last ~5 Myr with localization of relatively high strains within the Tararua Ranges [*Lamb and Vella*, 1987; *Nicol and Beavan*, 2003]. We suggest the high uplift rates within the ranges are the result of underplating further implying that the position of plate bending, and the locus of thrust faulting, has been sustained for the last 5 My; as suggested by *Nicol and Beavan* [2003].

8. Conclusions

In this study, we have developed a 2-dimensional P-wave velocity model across a 350 km long transect of the Hikurangi margin subduction zone beneath the Wellington region with the aim of determining properties of the locked subduction thrust that may fail in a future large earthquake. Our analysis uses a well-constrained first-arrival ray tracing inversion technique to model SAHKE active source onshore-offshore and onshore explosion data. In addition, we have used the tomography velocity model to migrate picked reflection events and stacked low-fold land explosion data to image subducting slab geometry and crustal structure.

We propose that plate convergence in the last 5 My has stacked imbricated sheets of sedimentary material from the top of the Hikurangi Plateau, on the overriding Pacific plate into the footwall of the Wairarapa fault, driving uplift of the Tararua Range, and may be acting as a seal trapping fluid in the oceanic crust. Reflections from the Wairarapa fault show it is a steeply dipping listric fault that appears to bound the upper surface of reflective low-velocity underplated sediment, and sole into where the plate interface intersects Australian Plate Moho at about 32 km depth and near the downdip end of the strongly locked coupled zone. The subducting oceanic crust is defined by a strong velocity gradient at 10 km depth offshore to the east but becomes less distinct beneath the Tararua Ranges where reflection data and seismicity infer an increase in dip at about 15 km depth from less than from 5° to greater than 15°. Bending stresses brought about by dehydration in the slab have likely reactivated widespread steeply dipping normal faults on the incoming plate expressed by vertical clusters in seismicity [*Du et al*., 2004]. Low P-wave velocities < 7.0 km/s in our velocity model, and high Vp/Vs [*Eberhart-Phillips and Reyners*, 2012] are consistent with high fluid pressure in the bend region. The bend in the plate is also marked by splay fault branching and a step down in the plate interface decollément that acts to

transfer slip to the top of the oceanic crust and allows low-velocity Cretaceous and Paleogene strata to be underplated.

Previously we have documented that there is a long-lived along strike change in dip of the Hikurangi subduction interface at 10–20 km depth that is spatially correlated with changes in surface slope and the pattern of sediment accretion, deformation, and underplating within the outer forearc crustal wedge [*Barker et al*., 2010]. We can now extend that correlation to the southern Hikurangi margin and further suggest that increase in dip to angles greater than 8° defines the transition from locked areas of the plate interface to unlocked and partitions stable and unstable slip regimes. As a result mechanical behavior and seismic hazard of the subduction interface may also be spatially correlated with this along-strike change of interface geometry, although steps in the plate interface appear to be no impediment to megathrust earthquakes.

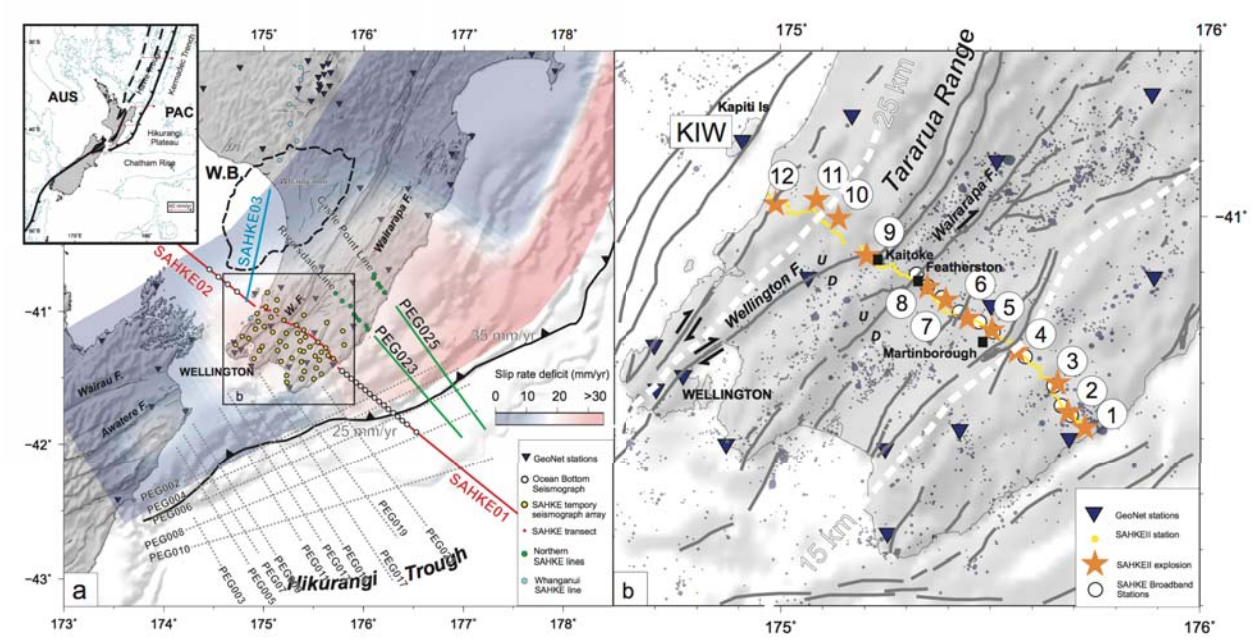

Figure 1. Tectonic setting showing major active faults of the southern North Island, of the southern North Island of New Zealand. (**a)** Coloured image show the slip rate deficit distribution at the plate interface [*Wallace et al.*, 2012]. Red regions are where the plate interfaced is locked. Gray dotted lines show the lines of the PEGASUS PEG09 survey which were recorded by the SAHKE array deployment (stations shown by yellow dots). The red lines are SAHKE01 and SAHKE02 recorded onshore by the transect deployment indicated by red dots. 20 Ocean bottom seismometers (white dots) were also deployed during this survey along SAHKE01 and SAHKE02. The blue line shows the offshore Wanganui line (SAHKE03), which was recorded by the associated blue stations onshore (WANGANUI line). The green lines (PEG023/PEG025) show the northernmost lines of the PEG09 survey, which were shot in mid-March and were recorded by two dedicated onshore seismic lines (Castlepoint line and Riversdale line). Inverted blue triangles indicate the locations of permanent stations which are part of the National Network and Wellington regional network monitored by GeoNet. Thin black lines denote active faults: W.F.=Wellington fault. The dashed black line is the -100 mGal Bouguer gravity anomaly and outlines the approximate extent of the Wanganui Basin (W.B.). Numbers indicate convergence rate at the Hikurangi Trough (in mm/yr) [*Wallace et al.*, 2012]. The inset shows the location of the study area where the Hikurangi Plateau (Pacific Plate - PAC) subducts beneath the east coast of North Island, New Zealand (Australian Plate - AUS) at the southern end of the Tonga-Kermadec subduction system. (**b)** Location of the seismometers (yellow points; spaced 50-100m apart) deployed during SAHKE II, and the (numbered) orange stars show the locations of the 12 borehole seismic sources. Green circles show the location of the broadband stations. White dashed lines show depth contours on the plate interface determined from relocated earthquakes [*Reyners and Eberhart-Phillips*, 2009]. The light blue dots show the location of relocated earthquakes [*Reyners et al.*, 2011] from 2001 to 2010; size of dots show the magnitude of the event. Grey lines show active faults, with U and D illustrating the up down sense of displacement.

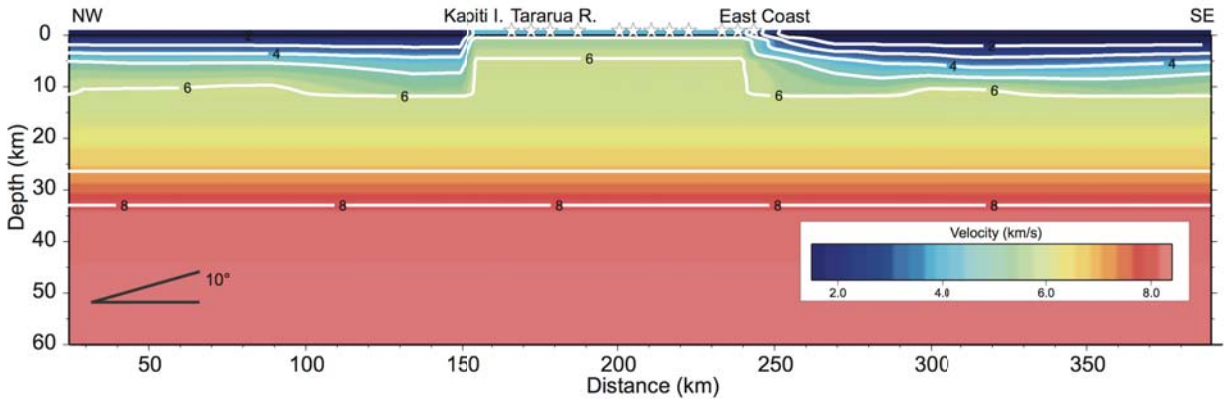

Figure 2. Starting regional velocity model. Offshore, this starting model accounts for bathymetry and sediment velocities. From the seabed to a depth of 8 km beneath the seabed, we fix our velocity model to a spatial average of velocities determined by optimal migration and stacking of MCS data.

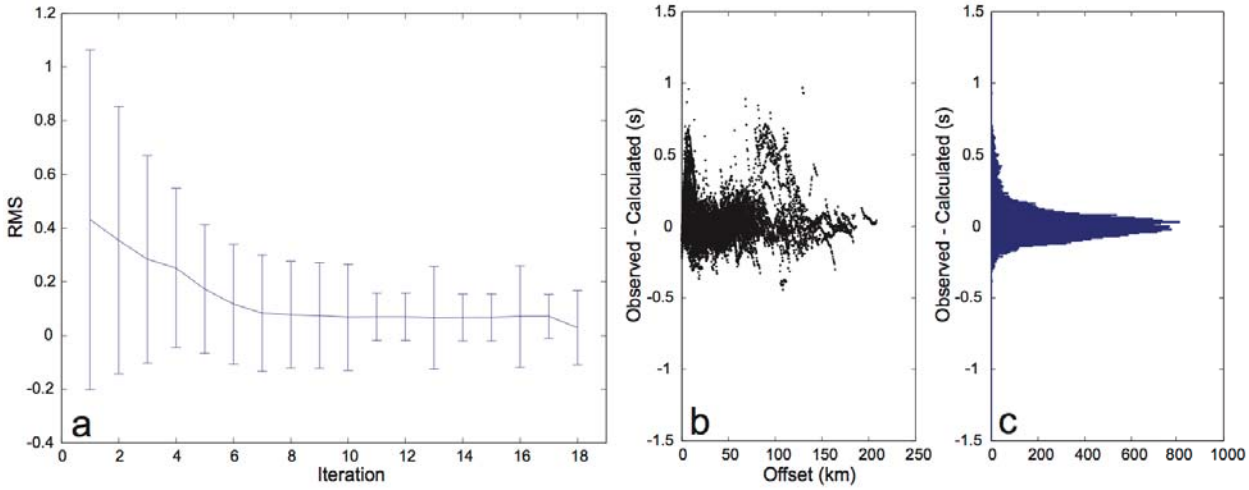

Figure 3. (a) RMS values for each iteration of first-arrival tomography. The vertical bar associated with each iteration is one standard deviation. The increase in RMS at iteration 13 and 16 correspond to grid refinements. (b) Traveltime residuals (observed – calculated) versus offset calculated for the final velocity model after 18 iterations. (c) Distribution of traveltime residuals corresponding to (b).

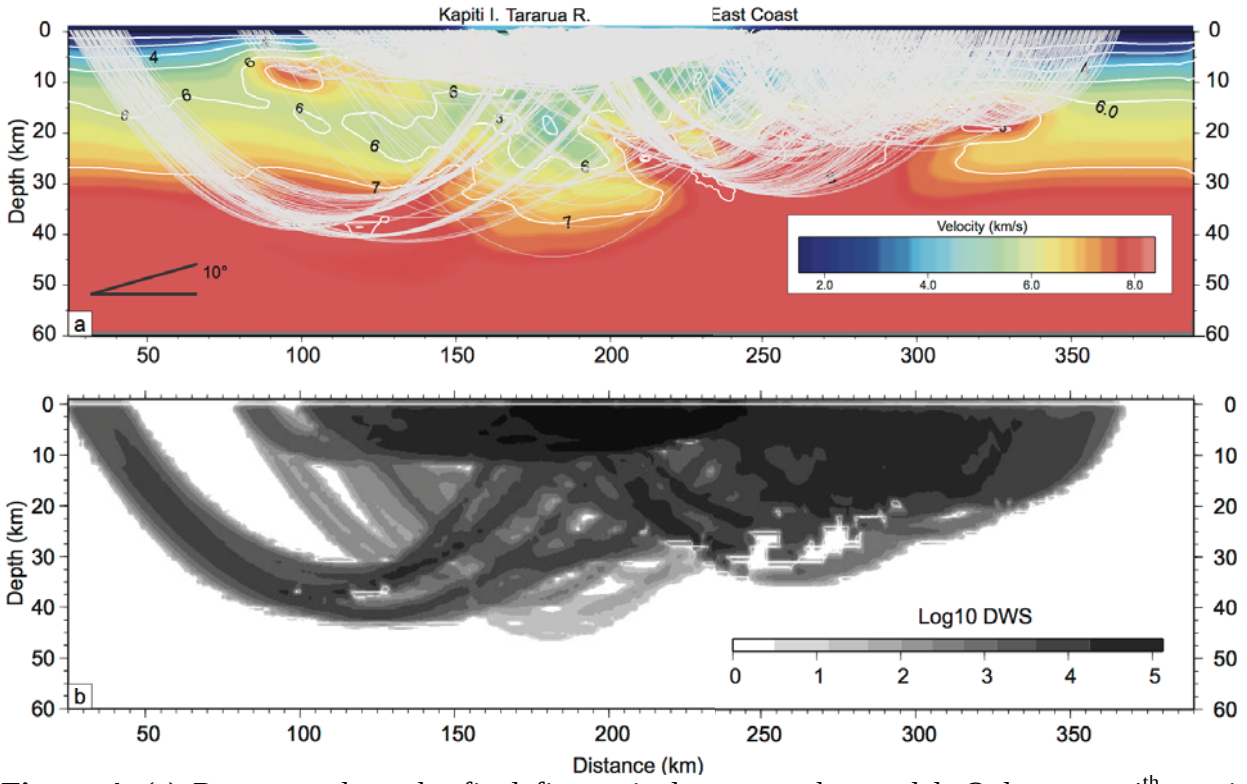

Figure 4. (a) Rays traced on the final first-arrival tomography model. Only every 4th ray is plotted. (b) Grid of derivative weight sum (DWS). The DWS weights each ray path length according to its spatial separation from the grid node. Larger DWS values indicate better data coverage.

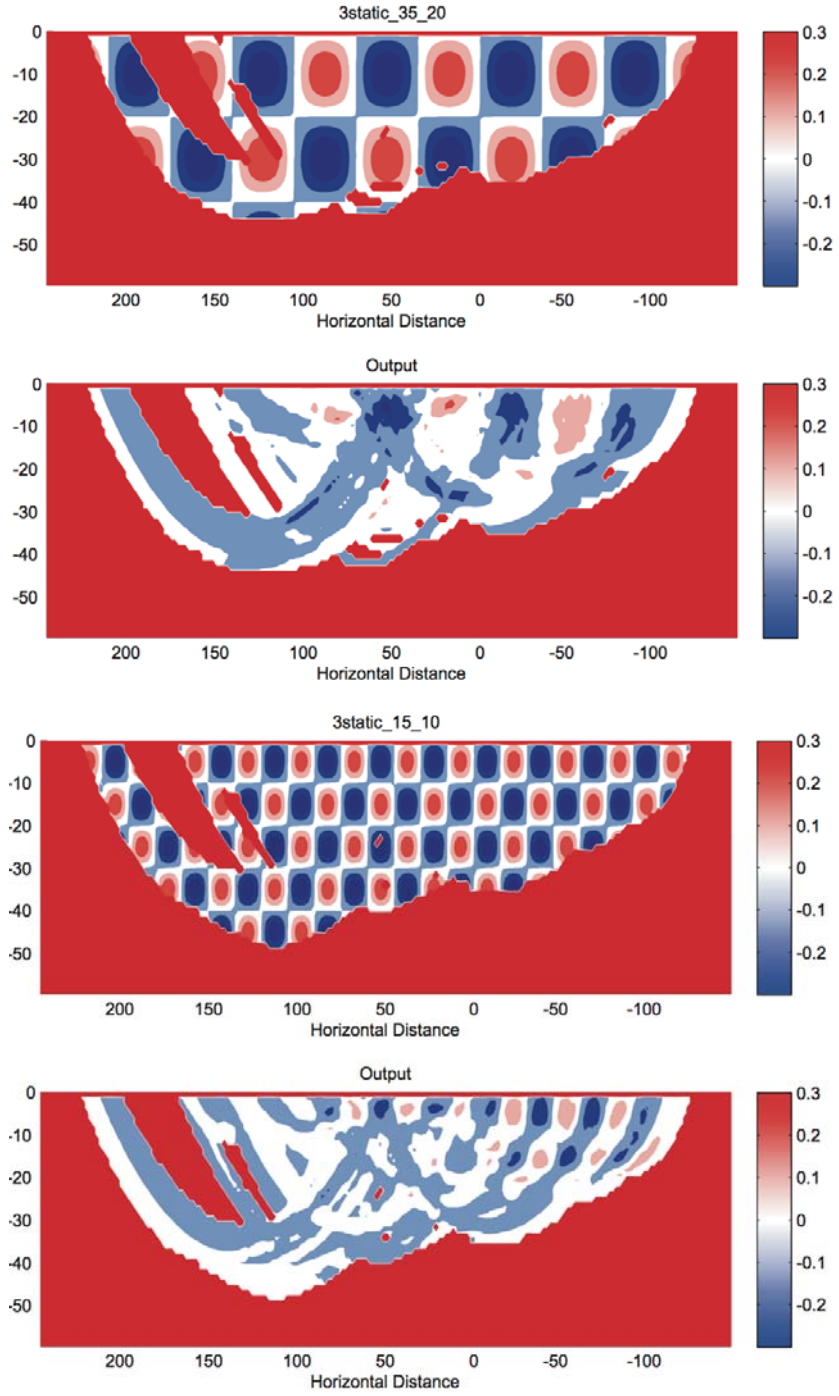

Figure 5. First-arrival tomography checkerboard resolutions tests using ±0.3 km/s perturbations. SAHKEII shot point localities designated as stars with shot 1 and 12 annotated. Starting (a and c) and recovered (b and d) anomaly patterns for cell sizes 35 x 20 km and 15 x 10 km respectively. Regions of high resolution are consistent with dense ray coverage and high DWS (Figure 4a and b)

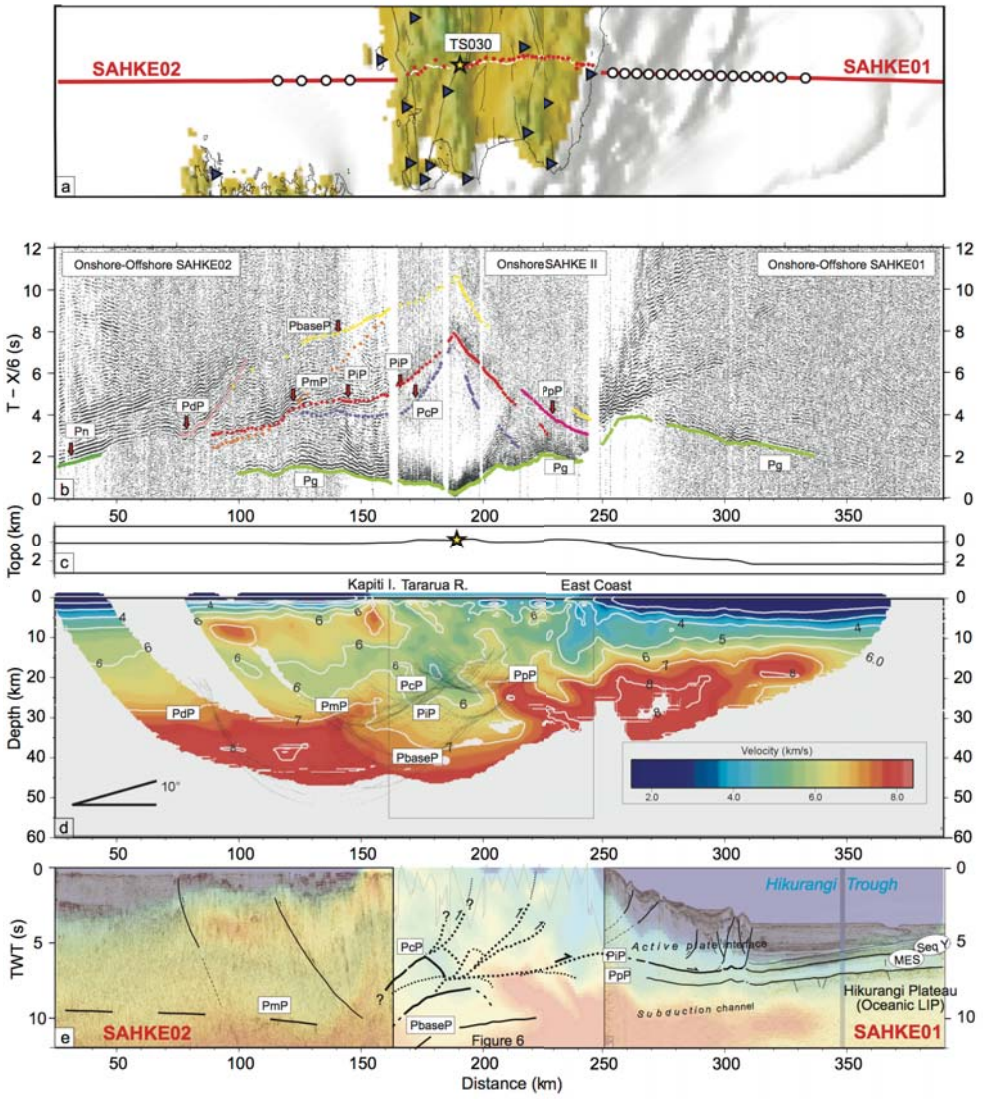

Figure 6. Composite plot of onshore-offshore gather at station TS030 and land shot 9. (a) SAHKE station location map with TS030/Shot 9 as yellow star. See Figure 1 for the key to symbols. (b) Combined gather produces a 350-km wide "supergather" (Okaya *et al.*, 2002) with identified phases observed on most transect supergathers. Pg samples the upper and lower crust (green) of the Pacific and Australian Plates and Pn (dark green) samples the Australian Plate upper mantle. Reflections PcP (violet), PintP (red), PtopP (pink), PbaseP (yellow) are phases associated with the Pacific Plate subducting crust. PmP reflections (orange) derive from the base of the Austrlan Plate crust and radiate diffractions (PdP – magenta). (c) SAHKE transect topography with shot point localities designated as stars and TS030/Shot 9 as the yellow filled star. (d) Vp structure using picked first-arrival Pg and Pn phases. The velocity model is masked where the DWS is less than 10. Superimposed on the model are stacked depth migrated picked reflection phases from (b). (e) Marine MCS (SAHKE01 and SAHKE02) data with the two-way-travel-time (twt) converted velocity model superimposed. Picked horizons and faults are shown in black and dashed where uncertain. The interpretation beneath the central section is from the low fold stack of land explosions [*Henrys et al.*, 2013].

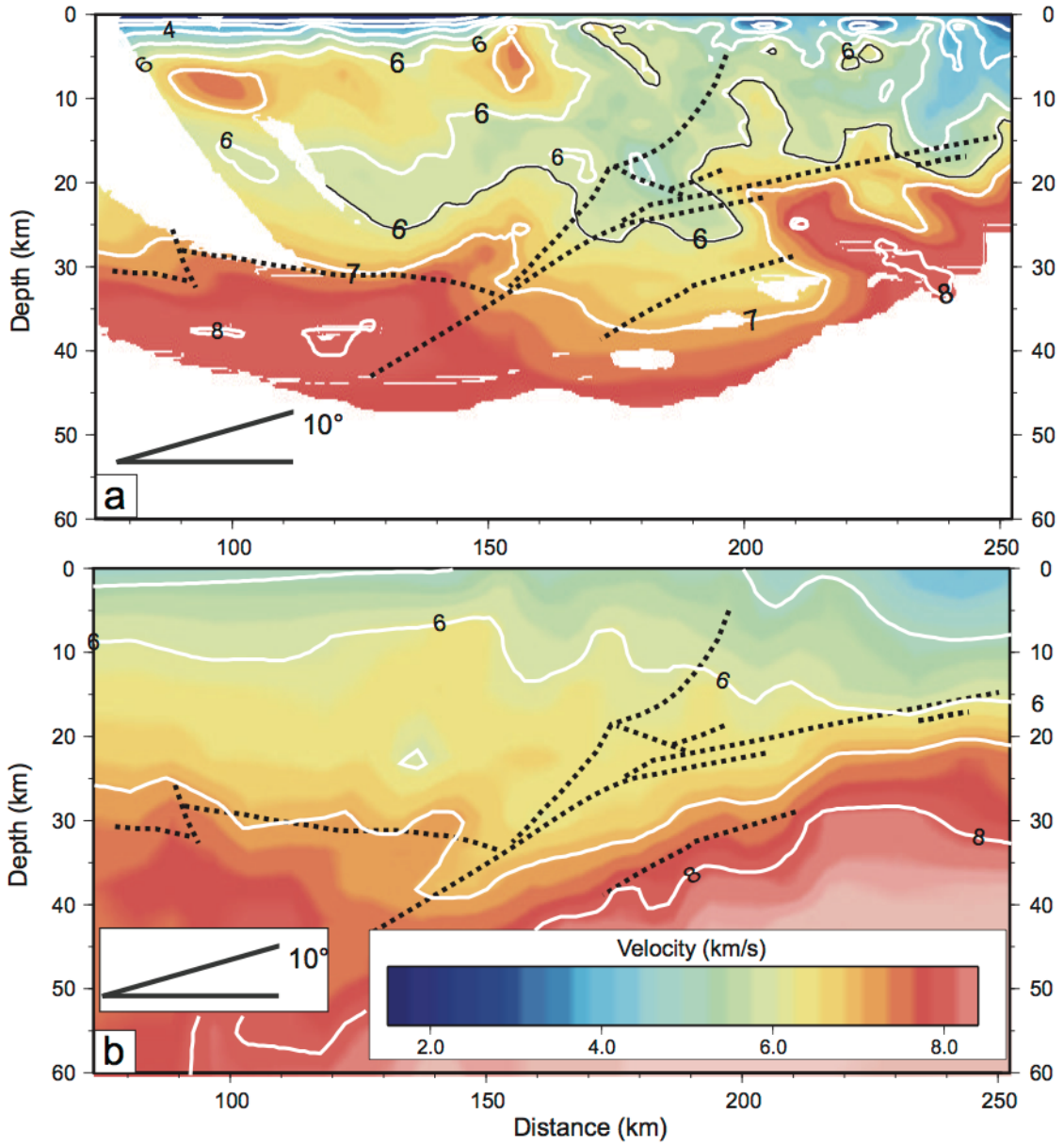

Figure 7. Comparison of (a) first-arrival tomography velocity model from Figure 3d to (b) co-located section from previously published 3-dimensional P-wave model of [*Eberhart-Phillips and Reyners*, 2012]. See text for comparative description of models. Both are plotted with the same color scale and have interpreted boundaries and faults (dashed black lines) determined from stacked migrated picks [*Henrys et al.*, 2013]. SAHKEII shot point localities designated as stars.

References:

Ammon, C. J., C. Ji, H.-K. Thio, D. Robinson, S. Ni, V. Hjorleifsdottir, H. Kanamori, T. Lay, S. Das, D. Helmberger, G. Ichinose, J. Polet, and D. Wald (2005), Rupture Process of the 2004 Sumatra-Andaman Earthquake, *Science*, *308*(5725), 1133-1139.

Barker, D. H., R. Sutherland, S. A. Henrys, and S. Bannister (2010), Geometry of the Hikurangi subduction thrust and upper plate, North Island, New Zealand, *Geochemistry, Geophysics, Geosystems*, *10*(2), Q02007.

Bassett, D., R. Sutherland, S. Henrys, T. Stern, M. Scherwath, A. Benson, S. Toulmin, and M. Henderson (2010), Three-dimensional velocity structure of the northern Hikurangi margin, Raukumara, New Zealand: Implications for the growth of continental crust by subduction erosion and tectonic underplating, *Geochem. Geophys. Geosyst.*, *11*(10), Q10013.

Calvert, A. J., L. A. Preston, and A. M. Farahbod (2011), Sedimentary underplating at the Cascadia mantle-wedge corner revealed by seismic imaging, *Nature Geosci*, *4*(8), 545-548.

Davy, B. R., K. Hoernle, and R. Werner (2008), The Hikurangi Plateau – crustal structure, rifted formation and Gonwana subduction history, *Geochemistry Geophysics Geosystems*, *9*, Q07004.

Du, W. X., C. H. Thurber, M. E. Reyners, D. Eberhart-Phillips, and H. Zhang (2004), New constraints on seismicity in the Wellington region of New Zealand from relocated earthquake hypocentres, *Geophysical Journal International*, *158(3)*, 1088-1102.

Eberhart-Phillips, D. (1990), Three-DimensionalP and S Velocity Structure in the CoalingaRegion, California, *Journal of Geophysical Research*, *95*(B10), 15343-15363.

Eberhart-Phillips, D. (1993), Local earthquake tomography : earthquake source regions, in *Seismic tomography : theory and practice.*, edited by H. M. Iyer and K. Hirahara, pp. 613-643, Chapman & Hall, London.

Eberhart-Phillips, D., and M. Reyners (2012), Imaging the Hikurangi Plate interface region, with improved local-earthquake tomography, *Geophysical Journal International*, *190*(2), 1221-1242, doi:10.1111/j.1365-246X.2012.05553.x.

Henrys, S. A., M. E. Reyners, I. A. Pecher, S. C. Bannister, Y. Nishimura, and G. Maslen (2006), Kinking of the subducting slab by escalator normal faulting beneath the North Island of New Zealand, *Geology*, *34*(9), 777-780, doi: 710.1130/G22594.22591.

Henrys, S., et al. (2013), SAHKE geophysical transect reveals crustal and subduction zone structure at the southern Hikurangi margin, New Zealand, *Geochem. Geophys. Geodyn. (G3)*(in review).

Kodaira, S., T. Iidaka, A. Kato, J.-O. Park, T. Iwasaki, and Y. Kaneda (2004), High pore fluid pressure may cause silent slip in the Nankai Trough, *Science*, *304*(5675), 1295-1298.

Lamb, S. H., and P. Vella (1987), The last million years of deformation in part of the New Zealand plate-boundary zone, *Journal of Structural Geology*, *9*(7), 877-891.

Lay, T., H. Kanamori, C. J. Ammon, M. Nettles, S. N. Ward, R. C. Aster, S. L. Beck, S. L. Bilek, M. R. Brudzinski, R. Butler, H. R. DeShon, G. Ekstrom, K. Satake, and S. Sipkin (2005), The Great Sumatra-Andaman Earthquake of 26 December 2004, *Science*, *308*(5725), 1127-1133.

Nicol, A., and J. Beavan (2003), Shortening of an overriding plate and its implications for slip on a subduction thrust, central Hikurangi Margin, New Zealand, *Tectonics*, *22*(6), 9-1 - 9-14.

Okaya, D., S. Henrys, and T. Stern (2002), Double-sided onshore-offshore seismic imaging of a plate boundary; "super-gathers" across South Island, New Zealand, *Tectonophysics*, *355*(1-4), 247-263.

Plaza-Faverola, A., D. Klaeschen, P. Barnes, I. A. Pecher, S. Henrys, and J. Mountjoy (2012), Evolution of fluid expulsion and concentrated hydrate zones across the southern Hikurangi subduction Margin, New Zealand: an analysis from depth migrated seismic data, *Geochem. Geophys. Geosyst.*, *13*, Q08018.

Reyners, M., and D. Eberhart-Phillips (2009), Small earthquakes provide insight into plate coupling and fluid distribution in the Hikurangi subduction zone, New Zealand, *Earth Planet. Sci. Lett.*, *282*(1-4), 299-305.

Reyners, M., D. Eberhart-Phillips, and S. Bannister (2011), Tracking repeated subduction of the Hikurangi Plateau beneath New Zealand, *Earth Planet. Sci. Lett.*, *311*(1-2), 165-171.

Savage, M. K., J. Park, and H. Todd (2007), Velocity and anisotropy structure at the Hikurangi subduction margin, New Zealand from receiver functions, *Geophysical Journal International*, *168*(3), 1034-1050.

Simons, M., S. E. Minson, A. Sladen, F. Ortega, J. Jiang, S. E. Owen, L. Meng, J.-P. Ampuero, S. Wei, R. Chu, D. V. Helmberger, H. Kanamori, E. Hetland, A. W. Moore, and F. H. Webb (2011), The 2011 Magnitude 9.0 Tohoku-Oki Earthquake: Mosaicking the Megathrust from Seconds to Centuries, *Science*, *332*(6036), 1421-1425.

Thurber, C., and D. Eberhart-Phillips (1999), Local earthquake tomography with flexible gridding, *Computers and Geosciences*, *25*, 809-818.

Toomey, D. R., and G. R. Foulger (1989), Tomographic inversion of local earthquake data from the Hengill-Grensdalur central volcano complex, Iceland, *Journal of Geophysical Research*, *94*(B12), 17497-17510, doi:10.1029/JB094iB12p17497.

Wallace, L. M., M. Reyners, U. Cochran, S. Bannister, P. M. Barnes, K. Berryman, G. Downes, D. Eberhart-Phillips, A. Fagereng, S. Ellis, A. Nicol, R. McCaffrey, R. J. Beavan, S. Henrys, R. Sutherland, D. H. N. Barker, N. Litchfield, J. Townend, R. Robinson, R. Bell, K. Wilson, and W. Power (2009), Characterizing the seismogenic zone of a major plate boundary subduction thrust: Hikurangi Margin, New Zealand, *Geochemistry Geophysics Geosystems*, *10*, 32.

Wallace, L. M., P. Barnes, J. Beavan, R. Van Dissen, N. Litchfield, J. Mountjoy, R. Langridge, G. Lamarche, and N. Pondard (2012), The kinematics of a transition from subduction to strike-slip: An example from the central New Zealand plate boundary, *J. Geophys. Res.*, *117*(B2), B02405.

PART II – Alpine Fault

Technical Abstract:

Tectonic tremor is characterized by persistent, low-frequency seismic energy seen at major plate boundaries. Although predominantly associated with subduction zones, tremor also occurs along the deep extension of the strike-slip San Andreas Fault. Here we present the first observations of tectonic tremor along New Zealand's Alpine Fault, a major transform boundary that is late in its earthquake cycle. We report tectonic tremor that occurred on the central section of the Alpine Fault on 12 days between March 2009 and October 2011. Tremor hypocenters concentrate in the lower crust at the downdip projection of the Alpine Fault; coincide with a zone of high P-wave attenuation (low Q_p) and bright seismic reflections; occur in the 25–45 km depth range, below the seismogenic zone; and may define the deep plate boundary structure extending through the lower crust and into the upper mantle. We infer this tremor to represent slow slip on the deep extent of the Alpine Fault in a fluid-rich region marked by high attenuation and reflectivity. These observations provide the first indication of present-day displacement on the lower crustal portion of the Australia–Pacific transform plate boundary.

1. Foreword

The following report is taken from the published manuscript:

Wech, A. G., C. M. Boese, T. A. Stern, and J. Townend (2012), Tectonic tremor and deep slow slip on the Alpine Fault, Geophys. Res. Lett., 39, L10303, doi:10.1029/2012GL051751.

2. Introduction

New Zealand straddles the boundary between the Australian and Pacific plates, whose collision has formed three distinct tectonic regimes spanning the country's two main islands. Beneath the North Island, this boundary is manifest as westward subduction of the Pacific plate at the Hikurangi Trough. At the southern end of the South Island, the subduction polarity is reversed, with the Australian plate subducting eastward. In between, collision gives rise to the Alpine Fault, a 650 km-long transform fault. This transpressional structure, which runs the length of the South Island, accommodates most of the relative motion between the two plates: approximately 21–27 mm/yr of the 37±2 mm/yr relative plate motion occurs as dextral slip on the Alpine Fault, with the remaining plate motion accommodated through uplift and auxiliary faulting [*Norris and Cooper*, 2001; *Sutherland et al.*, 2006].

This study focuses on the central portion of the Alpine Fault, whose role in relieving strain accumulation remains poorly understood [*Sutherland et al.*, 2007; *Walcott*, 1978]. Paleoseismic evidence suggests that the central Alpine Fault ruptures in M_w~7.9 earthquakes every 200–400 years and that it last ruptured in 1717 [*Sutherland et al.*, 2007]. Seismicity larger than M_L~2 is particularly sparse in the region [*Boese et al.*, 2012; *Evison*, 1971; *Leitner et al.*, 2001], the Alpine Fault exhibits no evidence for present-day creep at the surface (based on repeated geodetic observations and the lack of distorted cultural structures) [*Beavan et al.*, 1999; *Sutherland et al.*, 2007], and interpreted GPS measurements indicate that the fault is locked to a

depth of 13–18 km [*Wallace et al.*, 2007]. These observations and the time elapsed since the last major earthquake suggest that the Alpine Fault is late in its earthquake cycle, making any observations of seismic or aseismic deformation critical in refining current hazard estimates.

Tectonic tremor is an emergent, low-amplitude signal, that has durations of minutes to days and lacks the higher-frequency energy radiated by normal earthquakes [*Obara*, 2002]. First observed in subduction zones, tremor is often spatially and temporally correlated with geodetically observed slow slip [*Bartlow et al.*, 2011; *Obara et al.*, 2004]; however, this correlation can be complex [*Kim et al.*, 2011; *Peterson et al.*, 2011], and low-level tremor can occur without detectable slow slip [*Wech et al.*, 2009]. A growing body of evidence suggests that tectonic tremor is the seismic signature of slow slip [*Shelly et al.*, 2007; *Shelly et al.*, 2006; *Wech and Creager*, 2007], making tremor a useful tool in identifying slip below geodetic resolution [*Shelly and Johnson*, 2011; *Wech and Creager*, 2011]. On the San Andreas Fault—the only transform boundary where tremor has been observed—deep (20–40 km), low-level tremor occurs below a locked section of the fault [*Nadeau and Dolenc*, 2005]. This seismic signal occurs without any associated geodetic signal [*Johnston et al.*, 2006] and is inferred to reflect deep, slow shear in the brittle–ductile transition zone [*Nadeau and Dolenc*, 2005].

Here, we report on tectonic tremor occurring along the deeper extension of the central portion of the Alpine Fault. Our observations suggest that slow slip occurs within the mid- to lower-crust or upper mantle, relieving stress in the transition zone from brittle to ductile behavior along the transform boundary between the Pacific and Australian plates. As our only present-day indicator of active deformation on the Alpine Fault, tremor provides a unique means of documenting and elucidating ambient coupling and stress conditions along this portion the plate boundary.

3. Data & Observations

We overcome some of the inherent obstacles associated with identifying tremor using a combination of seismic data from New Zealand's permanent broadband GeoNet network [*Petersen et al.*, 2011] and the Southern Alps Microearthquake Borehole Array (SAMBA), a network of 11 short-period seismometers installed in 2–100 m-deep boreholes, that spans the central Alpine Fault (Fig. 1) [*Boese et al.*, 2012]. As tremor lacks impulsive arrivals, it is usually identified by searching for persistent, coherent energy recorded at several sites [*Kao and Shan*, 2004]. However, detecting such coherence is difficult at large distances because of the signals' low amplitudes. SAMBA's c, 60 km aperture and dense station spacing (with average inter-station distances of 8 and 16 km parallel and perpendicular to the strike of the Alpine Fault, respectively) make it easier to identify and locate the source of low-amplitude, emergent signals than using GeoNet alone (80–100 km station spacing).

We have performed a systematic search for tremor using continuous seismic data spanning the interval from March 2009 to October 2011. High noise levels produced by local seismicity or local geomorphic processes (e.g. rockfalls, glacier movement, icefalls etc.) precluded the use of an automated detection method, and we therefore undertook a manual search for tremor activity. The east components of data from all stations are band-pass filtered from 1–6 Hz, rectified into envelopes, smoothed using a 20 s low-pass filter, and decimated to 1 Hz. The resulting envelope functions are inspected visually to identify persistent, coherent signals.

The identified tremor windows are then reprocessed to determine hypocenters. All available data are filtered from 2–10 Hz (to take advantage of the observed tremor bandwidth), rectified into envelopes, low-pass filtered at 0.2 Hz, and decimated at 5 Hz. We separate each visually identified tremor window into individual bursts that are located systematically with a waveform envelope cross-correlation technique [*Wech and Creager*, 2008] using those channels with

normalized cross-correlation values of >0.7. This method introduces epicentral uncertainties of approximately 8 km, but the alternative approach of cross-correlating smoothed envelopes provides poor depth constraints, which are exacerbated here by the tremor's occurrence outside the SAMBA network. Magnitudes have been calculated by calibrating the maximum amplitude of the signal at each station with those determined for earthquakes, which have in turn been calibrated to the GeoNet catalog [*Boese et al.*, 2012].

During the 2.5 years examined, we find 12 days on which tremor activity occurred and locate 65 individual bursts (Figure S1). Most of the tremor occurs beneath the Copland Valley on the southern edge of the SAMBA station network and extends ~30 km further to the southwest (Fig. 1). The 25–45 km-deep tremors (Fig. 3) form a near-vertical band that is subparallel to but offset southeastward from the trace of the Alpine Fault by about 15 km (Figs 1 & 2). The tremor bursts collectively occur in isolated sequences limited to durations of ~5–30 minutes and are equivalent in amplitude to M_L 1 earthquakes. Activity repeats irregularly with a few days to several months between individual tremor sequences. Because envelope cross-correlation techniques provide poor depth control, the tremor depths are not well constrained. Some tremor appears to extend into the upper mantle; but the apparent deepening of tremor to the southwest (Fig. 1) may be an artifact resulting from poor station coverage, and the 15 km depth uncertainty does not preclude tremor being restricted to the mid- to lower-crust. The tremor's location with respect to the SAMBA network decreases resolution and makes it difficult to employ other techniques for constraining depths and source process. Both inter-channel cross-correlation [*La Rocca et al.*, 2009] and tremor polarization [*Wech and Creager,* 2007] yield results that are difficult to interpret due to poor station coverage directly above the tremor.

The tremor we have identified represents the largest, most discernable examples of tremor activity in the region. It is likely that lower-level ambient tremor also occurs. However, as the durations of individual bursts get smaller, tremor becomes more difficult to detect, and distinguishing short-duration tremor from the geomorphic background noise, such as landslides and ice movement, emanating from the Southern Alps presents an additional challenge. Mainshock-aftershock sequences from the Dusky Sound, Darfield and Christchurch earthquakes also reduced tremor detectability for months at a time. Overall, the observed tremor activity occurs in infrequent, random, isolated sequences, and does not appear to correlate with appreciable increases or decreases in either the regional seismicity or microseismicity recorded by SAMBA [*Boese et al.*, 2012]. We do, however, note the occurrence of pronounced tremor activity just before the Dusky Sound earthquake [*Beavan et al.*, 2010; *Fry*, 2009]: in the 24 hours leading up to 50 minutes before that event, we recorded two distinct sequences of tremor. This occurrence is possibly coincidental, but its timing relative to the Dusky Sound earthquake warrants mention.

4. Discussion

4.1 Plate boundary at depth

At plate boundaries worldwide, tremor is inferred to be associated with slow shear-slip failure in the transition zone between stick slip and stable sliding of a fault [*Shelly et al.*, 2006; *Shelly et al.*, 2009; *Wech and Creager*, 2007]. Although our ability to resolve the depth and source process of tremor occurring in the vicinity of the Alpine Fault is limited by its position outside the SAMBA network, we interpret the tremor signals detected to represent slow shear failure at depth. Even given the large depth uncertainties, tremor hypocenters suggest that: 1) the majority of tremor occurs deeper than 25 km, below the geodetically inferred locked portion of the fault (Fig. 3); 2)

tremor and earthquakes are anti-correlated in depth, with a gap in between (Fig 3); and 3) the tremor possibly extends to depths as great as 45 km, potentially defining a deeper sub-vertical lineation that may distinguish itself from the 45–60° dip of the Alpine Fault (Fig. 2). Most of the tremor occurs at depths of ~30 km, which would place slow slip on the deep extension of the Alpine Fault (Figs. 2 & 3). The depth uncertainties limit our ability to make reliable geometrical inferences; however, if the deeper tremor hypocenters are real, then tremor may not solely represent slip on the Alpine Fault, but could also incorporate slip on a near-vertical, structure defining the plate boundary at depth. In contrast, the highly reflective, southeast-dipping boundary seen in seismic reflection data (Fig. 2) may represent a localized décollement surface between the lower and upper crust of the Pacific plate. Although the tremor likely represents plate boundary slip of some form, determining the slip geometry requires more precise depth analysis using, for example, low-frequency earthquakes comprising the tremor [*Shelly et al.*, 2009].

4.2 Presence of fluids

Slow slip is often spatially correlated with regions of elevated fluid content [*Audet et al.*, 2009; *Kodaira et al.*, 2004; *Song et al.*, 2009] and has been interpreted to be a fluid-related process. The three-dimensional P-wave attenuation ($1/Q_p$) structure determined from analysis of local earthquakes suggests that fluids may also be present in the tremor region beneath the Alpine Fault [*Eberhart-Phillips et al.*, 2008]. Tremor extends downwards from the base of the seismogenic zone and overlaps with a high-attenuation zone below a depth of 25 km (Fig. 2). This 10 km-thick, low-Q_p region exhibits the highest attenuation in the whole of South Island; *Eberhart-Phillips et al.* [2008] attributed it to the downdip extension of the Alpine Fault, with the high attenuation interpreted as an indicator for metamorphic fluids within a high-strain zone.

Tomographic models also indicate lower P-wave velocities in the area [*Eberhart-Phillips*, 2002], but these are not as well resolved as the attenuation structure. However, the 2D velocity structure obtained by inverting active source data from the South Island GeopHysical Transect line 2 (SIGHT T2) [*Scherwath*, 2003] reveals a low-velocity zone (Fig. 3) located above a zone of high-reflectivity inferred from a migrated seismic reflection profile, CDP'98 (Fig. 2) [*Stern et al.*, 2001; *Stern et al.*, 2007]. These bright seismic reflections have been interpreted to represent interconnected fluids at lithostatic pressures produced by metamorphic dewatering of the crustal root [*Stern et al.*, 2007] and coincide with both the tremor hypocenters and the region of high attenuation (Fig. 2). We cannot determine the spatial relationship between tremor and velocity or attenuation structure further south, but given the northward increase in network density, we are confident that no significant tremor of comparable duration or equivalent magnitude occurred north of the region of high attenuation during this study period.

A low-frequency signal emanating from a zone of high attenuation raises questions about path effects and the true nature of the tremor signal at its source. High attenuation can affect the frequency content of seismic signals, including tremor [*Gomberg et al.*, 2012], making any distinction between tremor and overlapping low-frequency or normal earthquakes difficult. However, the tremor is anti-correlated with local seismicity (Fig. 3), and even if it did represent an attenuated earthquake signal, the durations suggest overlapping events that might be best explained as repeated failure in response to loading from aseismic slip on the surrounding fault plane.

4.3 Fluid-weakened fault

It is unclear what role fluids play in generating tremor or enabling slow slip. Nor is it entirely certain that the association of the tremor with a zone of high attenuation means that fluids play a

significant role here. This observation is nevertheless consistent with the hypothesis that slip is enabled by low effective stress resulting from high fluid pressure [*Audet et al.*, 2009; *Kodaira et al.*, 2004], and it could explain the absence of tremor to the north. On the San Andreas Fault, tremor is correlated with small (<1 kPa), tidal-induced stresses, providing evidence of near-lithostatic pore pressures [*Thomas et al.*, 2009]. There, tremor occurs at similar depths [*Becken et al.*, 2011; *Nadeau and Guilhem*, 2009; *Shelly*, 2010; *Shelly and Johnson*, 2011] and temperatures [*Fagereng and Diener*, 2011; *Toy et al.*, 2010] to those estimated here and is similarly limited in duration [*Nadeau and Dolenc*, 2005] compared with tremor observed in the Cascadia or Nankai subduction zones where durations span a continuum from hours to months [*Obara et al.*, 2010; *Wech and Creager*, 2011]. In the absence of direct measurements of fluid pressure deep beneath the Southern Alps, the existence of high-pressure fluids is inferred from low P-wave speeds, attenuation structure and high seismic reflectivity. However, the coincidence of tremor and inferred fluids and the similarities between Alpine Fault tremor and San Andreas Fault tremor suggest that an analogous interpretation might be applicable to the Alpine Fault. We therefore propose that tremor is illuminating slip occurring on the deeper, fluid-weakened extent of the plate boundary.

There are, however, alternative explanations for the tremor we observe. Though slightly deeper, the detected tremor may represent slip on the inferred array of deep (>20 km) backshears within the hanging wall of the Alpine Fault [*Wightman and Little*, 2007]. Furthermore, slip could be localized to a region of high strain resulting from an along-strike change in fault geometry. While coincident with geophysical indicators of fluids at depth, tremor epicenters also correlate spatially with an inferred change in the dip of the Alpine Fault. Structural data suggest that the fault in this region undergoes a northeastward steepening in dip by 15–20° [*Little et al.*, 2005]. A

resulting zone of localized high strain from transitional fault geometry may account for the occurrence of tremor beneath the Copland Valley section of the fault and its apparent absence to the northeast. An extension of the SAMBA array to the south is needed to test this.

5. Implications

The Alpine Fault tremor observation expands our evidence of deep slip on transform faults beyond the San Andreas Fault and may improve understanding of the underlying physics by providing additional constraints on the conditions required for tremor and slip generation. For the Alpine Fault, the finding facilitates the use of tremor as a tool for investigating ambient conditions within the fault zone. It enables future studies to explore stress conditions and fault properties through studies of tidal [*Thomas et al.,* 2009] and earthquake [*Peng et al.,* 2009] triggering. More importantly, it means the fault is currently active at depth. While slow slip itself is innocuous, any such slip will redistribute stress in the vicinity and may increase of the load on neighboring fault patches. This static stress transfer from slow slip has been inferred in Cascadia [*Wech and Creager*, 2011] as well as along the San Andreas Fault [*Shelly and Johnson*, 2011] and could result in seismogenic triggering, either on the Alpine Fault or an adjacent fault. Finally, the observation raises the question about the depth extent of a future Alpine Fault rupture. The tremor observations obtained to date, while sparse, enable us to infer that semi-brittle behavior extends to depths greater than either the seismogenic 10–15 km cut-off of microseismicity (10–15 km; *Boese et al*., 2012) or the geodetically inferred locked zone (c. 18 km; *Wallace et al.*, 2007). Refined tremor depths may elucidate the interseismic relationship between tremor, microearthquakes, and large-scale locking, providing insight into rheological controls on coseismic rupture distribution.

6. Conclusions

We observe deep seismic tremor occurring along the Alpine Fault transform boundary between the Australian and Pacific plates. Tremor is spatially correlated with the inferred downdip extension of the Alpine Fault, high P-wave attenuation (low Q_p), and high seismic reflectivity in the crust. We attribute this tremor to fluid-enabled slow slip occurring below the seismogenic zone mainly in the lower crust, but possibly the very top of the upper mantle. This discovery marks both the first documentation of tremor associated with the Alpine Fault and the first indication of contemporary deep-slip on the plate boundary in southwestern New Zealand. Understanding deep slow slip is critical for our ability to fully characterize the conditions, dynamics and hazards of a locked fault late in its earthquake cycle.

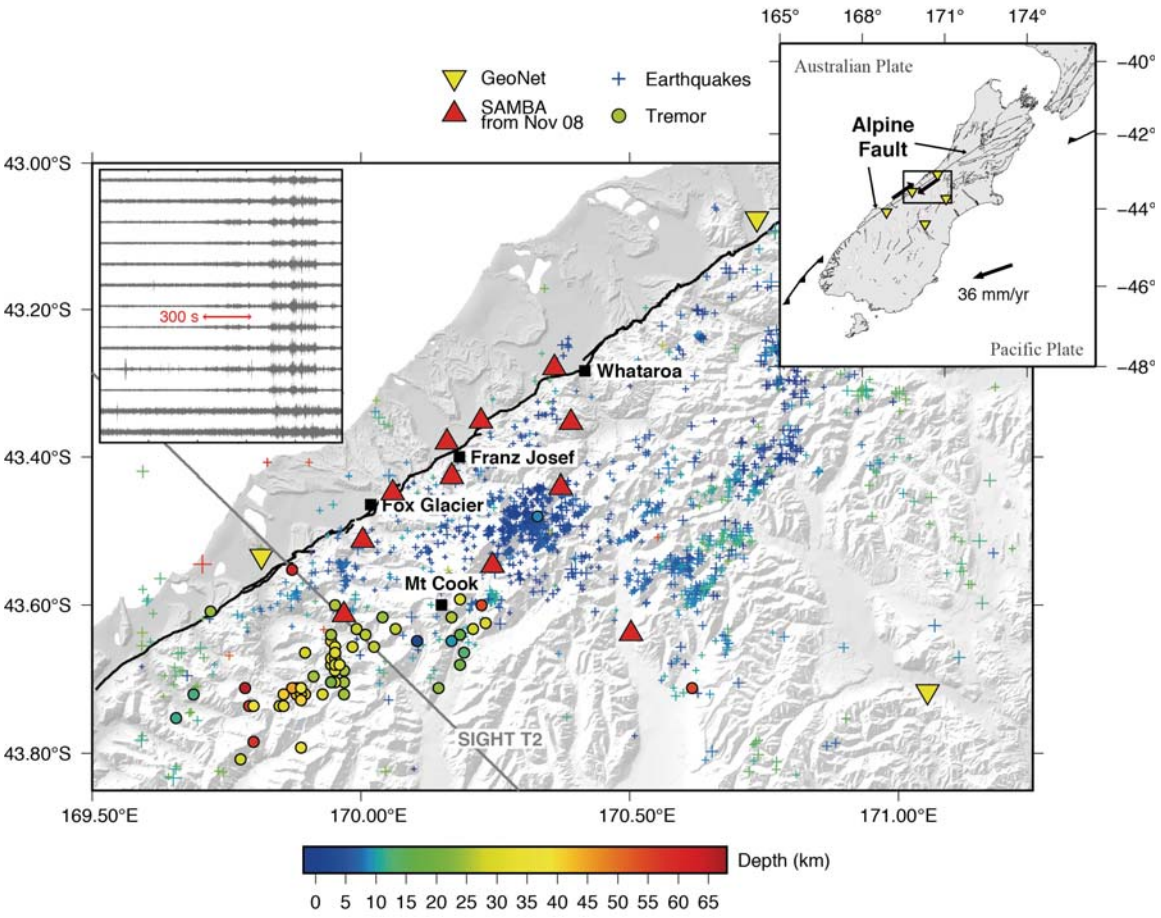

Figure 1. Earthquakes (crosses) and tremor locations (dots), color-coded with depth. Red and yellow triangles denote SAMBA and GeoNet seismic stations used in this study, respectively. The Alpine Fault trace is shown in black. Upper left inset shows 25 minutes of filtered horizontal-component seismograms (starting at 16:40 on 14 July 2010) containing tremor, recorded at 13 stations (10 SAMBA and the three western-most GeoNet stations) ordered by latitude. The SIGHT T2 (gray line) transect is shown through the tremor region.

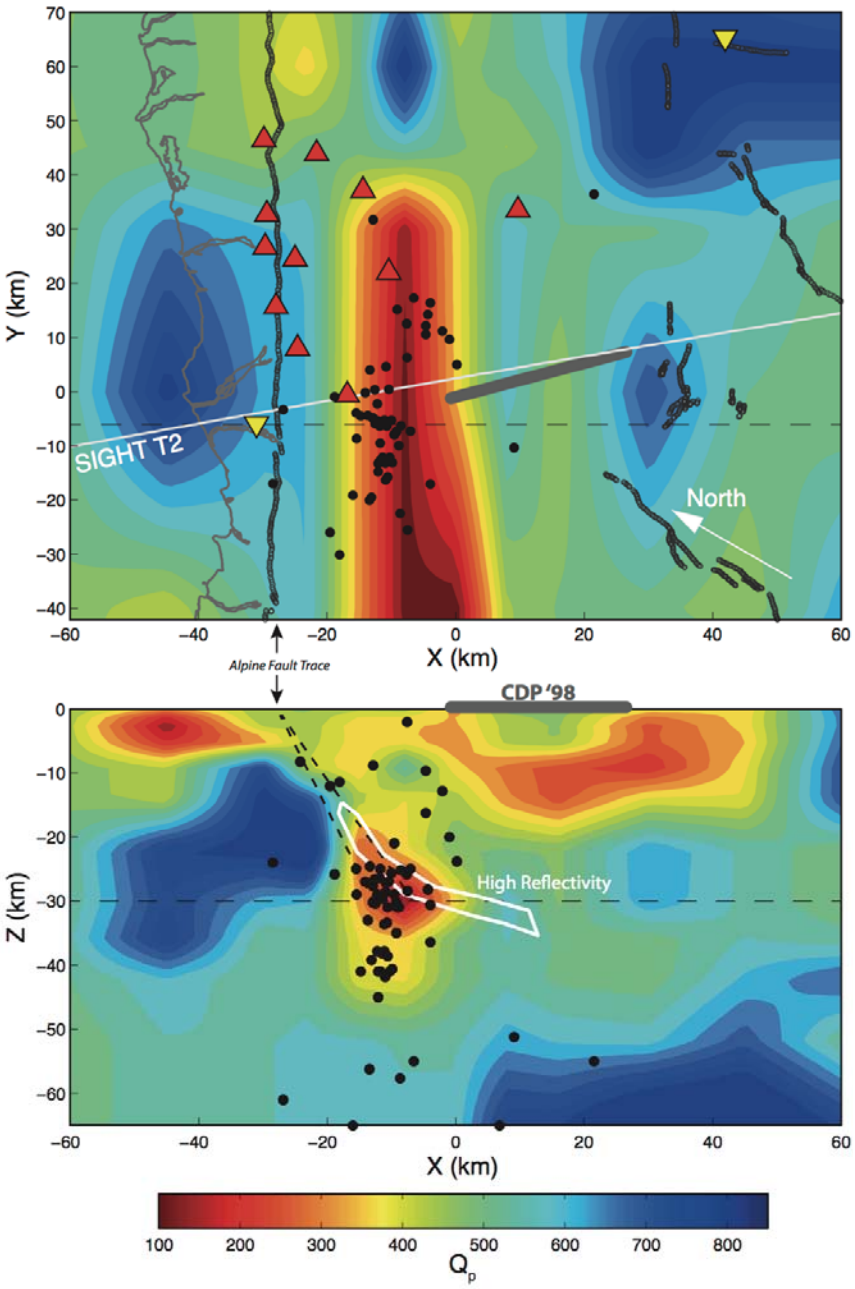

Figure 2. Tremor (black dots) and Q_p from regional tomography [*Eberhart-Phillips et al.*, 2008]. Low Qp = high attenuation. Top panel shows horizontal section at 30 km depth. SIGHT T2 transect is shown in white. Major fault traces in black. The dashed line marks the position of the cross-section illustrated in the bottom panel. Bottom panel shows profile through tremor region at Y= –6 km. The white area outlines a region of high reflectivity observed in the migrated CDP'98 reflection profile (grey line in both panels) [*Stern et al.*, 2007]. The two lines emanating from the Alpine Fault trace depict 45°- and 60°-dipping faults.

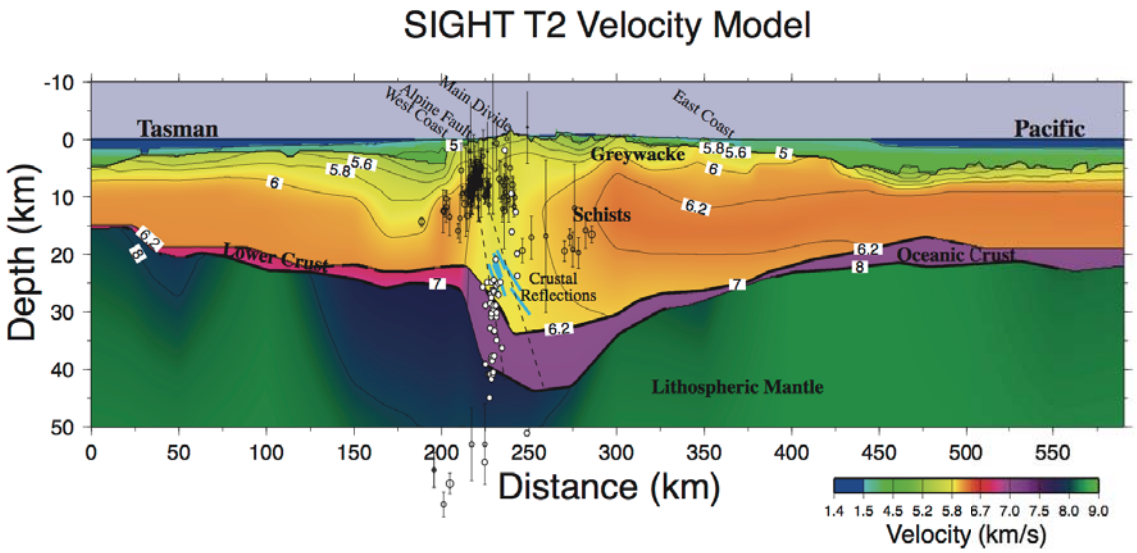

Figure 3. Local seismicity (black circles with depth uncertainty) and tremor (white circles) within 10 km (note difference from tremor in Figure 2) of the SIGHT T2 transect are shown on top of the preferred velocity model and interpretation [*Stern et al.*, 2007]. Region of high reflectivity from CPD'98 [*Stern et al.*, 2007] is shown as blue lines and dashed lines represent 45°- and 60°-dipping faults. Tremor is anti-correlated with earthquake seismicity and occurs below the low-velocity zone at the deeper extension of the Alpine Fault. The apparent westward dip in tremor hypocenters in this cross-section is an artifact stemming from a slightly skewed projection relative to the Alpine Fault trace (see Fig. 2) and vertical exaggeration.

References:

Audet, P., M. G. Bostock, N. I. Christensen, and S. M. Peacock (2009), Seismic evidence for overpressured subducted oceanic crust and megathrust fault sealing, *Nature*, *457*, 76-78, doi:10.1038/nature07650.

Bartlow, N. M., S. Miyazaki, A. M. Bradley, and P. Segall (2011), Space-time correlation of slip and tremor during the 2009 Cascadia slow slip event, *Geophys. Res. Lett.*, *38*, L18309, doi:10.1029/2011gl048714.

Beavan, J., S. Samsonov, P. Denys, R. Sutherland, N. Palmer, and M. Denham (2010), Oblique slip on the Puysegur subduction interface in the 2009 July MW 7.8 Dusky Sound earthquake from GPS and InSAR observations: implications for the tectonics of southwestern New Zealand, *Geophysical Journal International*, *183*, 1265-1286, doi:10.1111/j.1365-246X.2010.04798.x.

Beavan, J., et al. (1999), Crustal deformation during 1994-1998 due to oblique continental collision in the central Southern Alps, New Zealand, and implications for seismic potential of the Alpine fault, *J. Geophys. Res.*, *104*, 25233-25255, doi:10.1029/1999jb900198.

Becken, M., O. Ritter, P. A. Bedrosian, and U. Weckmann (2011), Correlation between deep fluids, tremor and creep along the central San Andreas fault, *Nature*, *480*, 87-90, doi:10.1038/nature10609.

Boese, C. M., J. Townend, E. Smith, and T. Stern (2012), Microseismicity and stress in the vicinity of the Alpine Fault, central Southern Alps, New Zealand, *J. Geophys. Res.*, *117*, B02302, doi:10.1029/2011jb008460.

Eberhart-Phillips, D. (2002), Three-dimensional crustal structure in the Southern Alps region of New Zealand from inversion of local earthquake and active source data, *J. Geophys. Res.*, *107*, 2262, doi:10.1029/2001jb000567.

Eberhart-Phillips, D., M. Chadwick, and S. Bannister (2008), Three-dimensional attenuation structure of central and southern South Island, New Zealand, from local earthquakes, *J. Geophys. Res.*, *113*, B05308, doi:10.1029/2007jb005359.

Evison, F. F. (1971), Seismicity of the Alpine Fault, New Zealand, *Recent crustal movements, Royal Society of New Zealand Bulletin*, *9*, 161-165.

Fagereng, Å., and J. F. A. Diener (2011), San Andreas Fault tremor and retrograde metamorphism, *Geophys. Res. Lett.*, *38*, L23303, doi:10.1029/2011gl049550.

Fry, B. (2009), The MW 7.6 Dusky Sound earthquake of 2009: Preliminary report, *Bull. N. Z. Soc. Earthq. Eng.*, *43*, 24-40.

Gomberg, J., K. C. Creager, J. R. Sweet, J. Vidale, A. Ghosh, and A. J. Hotovec (2012), Earthquake spectra and near-source attenuation in the Cascadia subduction zone, *in review*.

Johnston, M. J. S., R. D. Borcherdt, A. T. Linde, and M. T. Gladwin (2006), Continuous Borehole Strain and Pore Pressure in the Near Field of the 28 September 2004 M 6.0 Parkfield,

California, Earthquake: Implications for Nucleation, Fault Response, Earthquake Prediction, and Tremor, *Bulletin of the Seismological Society of America*, *96*, S56-S72, doi:10.1785/0120050822.

Kao, H., and S.-J. Shan (2004), The Source-Scanning Algorithm: mapping the distribution of seismic sources in time and space, *Geophysical Journal International*, *157*, 589-594, doi:10.1111/j.1365-246X.2004.02276.x.

Kim, M. J., S. Y. Schwartz, and S. Bannister (2011), Non-volcanic tremor associated with the March 2010 Gisborne slow slip event at the Hikurangi subduction margin, New Zealand, *Geophys. Res. Lett.*, *38*, L14301, doi:10.1029/2011gl048400.

Kodaira, S., T. Iidaka, A. Kato, J.-O. Park, T. Iwasaki, and Y. Kaneda (2004), High Pore Fluid Pressure May Cause Silent Slip in the Nankai Trough, *Science*, *304*, 1295-1298, doi:10.1126/science.1096535.

La Rocca, M., K. C. Creager, D. Galluzzo, S. Malone, J. E. Vidale, J. R. Sweet, and A. G. Wech (2009), Cascadia Tremor Located Near Plate Interface Constrained by S Minus P Wave Times, *Science*, *323*, 620-623, doi:10.1126/science.1167112.

Leitner, B., D. Eberhart-Phillips, H. Anderson, and J. L. Nabelek (2001), A focused look at the Alpine fault, New Zealand: Seismicity, focal mechanisms, and stress observations, *J. Geophys. Res.*, *106*, 2193-2220, doi:10.1029/2000jb900303.

Little, T. A., S. Cox, J. K. Vry, and G. Batt (2005), Variations in exhumation level and uplift rate along the obliqu-slip Alpine fault, central Southern Alps, New Zealand, *Geological Society of America Bulletin*, *117*, 707, doi:10.1130/b25500.1.

Nadeau, R. M., and D. Dolenc (2005), Nonvolcanic tremors deep beneath the San Andreas fault, *Science*, *307*, 389, doi:10.1126/science.1107142.

Nadeau, R. M., and A. Guilhem (2009), Nonvolcanic Tremor Evolution and the San Simeon and Parkfield, California, Earthquakes, *Science*, *325*, 191-193, doi:10.1126/science.1174155.

Norris, R. J., and A. F. Cooper (2001), Late Quaternary slip rates and slip partitioning on the Alpine Fault, New Zealand, *Journal of Structural Geology*, *23*, 507-520, doi:10.1016/s0191-8141(00)00122-x.

Obara, K. (2002), Nonvolcanic deep tremor associated with subduction in southwest Japan, *Science*, *296*, 1679-1681, doi:10.1126/science.1070378.

Obara, K., H. Hirose, F. Yamamizu, and K. Kasahara (2004), Episodic slow slip events accompanied by non-volcanic tremors in southwest Japan subduction zone, *Geophys. Res. Lett.*, *31*, L23602, doi:10.1029/2004GL020848.

Obara, K., S. Tanaka, T. Maeda, and T. Matsuzawa (2010), Depth-dependent activity of non-volcanic tremor in southwest Japan, *Geophys. Res. Lett.*, *37*, L13306, doi:10.1029/2010gl043679.

Peng, Z. G., J. E. Vidale, A. G. Wech, R. M. Nadeau, and K. C. Creager (2009), Remote triggering of tremor along the San Andreas Fault in central California, *J. Geophys. Res.*, *114*, B00A06, doi:10.1029/2008jb006049.

Petersen, T., K. Gledhill, M. Chadwick, N. H. Gale, and J. Ristau (2011), The New Zealand National Seismograph Network, *Seismological Research Letters, 82*(1), 9-20, doi: 10.1785/gssrl.82.1.9.

Peterson, C. L., S. R. McNutt, and D. H. Christensen (2011), Nonvolcanic Tremor in the Aleutian Arc, *Bulletin of the Seismological Society of America*, *101*, 3081-3087, doi:10.1785/0120100241.

Scherwath, M. (2003), Lithospheric structure across oblique continental collision in New Zealand from wide-angle P wave modeling, *J. Geophys. Res.*, *108*, 2566, doi:10.1029/2002jb002286.

Shelly, D. R. (2010), Migrating tremors illuminate complex deformation beneath the seismogenic San Andreas fault, *Nature*, *463*, 648-652, doi:10.1038/nature08755.

Shelly, D. R., and K. M. Johnson (2011), Tremor reveals stress shadowing, deep postseismic creep, and depth-dependent slip recurrence on the lower-crustal San Andreas fault near Parkfield, *Geophys. Res. Lett.*, *38*, L13312, doi:10.1029/2011gl047863.

Shelly, D. R., G. C. Beroza, and S. Ide (2007), Non-volcanic tremor and low-frequency earthquake swarms, *Nature*, *446*, 305-307, doi:10.1038/nature05666.

Shelly, D. R., G. C. Beroza, S. Ide, and S. Nakamula (2006), Low-frequency earthquakes in Shikoku, Japan, and their relationship to episodic tremor and slip, *Nature*, *442*, 188-191, doi:10.1038/nature04931.

Shelly, D. R., W. L. Ellsworth, T. Ryberg, C. Haberland, G. S. Fuis, J. Murphy, R. M. Nadeau, and R. Burgmann (2009), Precise location of San Andreas Fault tremors near Cholame, California using seismometer clusters: Slip on the deep extension of the fault?, *Geophys. Res. Lett.*, *36*, L01303, doi:10.1029/2008gl036367.

Song, T. R. A., D. V. Helmberger, M. R. Brudzinski, R. W. Clayton, P. Davis, X. Perez-Campos, and S. K. Singh (2009), Subducting Slab Ultra-Slow Velocity Layer Coincident with Silent Earthquakes in Southern Mexico, *Science*, *324*, 502-506, doi:10.1126/science.1167595.

Stern, T., S. Kleffmann, D. Okaya, M. Scherwath, and S. Bannister (2001), Low seismic-wave speeds and enhanced fluid pressure beneath the Southern Alps of New Zealand, *Geology*, *29*, 679-682, doi:10.1130/0091-7613(2001)029<0679:lswsae>2.0.co;2.

Stern, T., D. Okaya, S. Kleffmann, M. Scherwath, S. Henrys, and F. Davey (2007), Geophysical Exploration and Dynamics of the Alpine Fault Zone, in *Tectonics at South Island, New Zealand*, edited by D. Okaya, T. Stern and F. Davey, pp. 207–233, AGU Geophysical Monograph Series.

Sutherland, R., K. Berryman, and R. Norris (2006), Quaternary slip rate and geomorphology of the Alpine fault: Implications for kinematics and seismic hazard in southwest New Zealand, *Geological Society of America Bulletin*, *118*, 464-474, doi:10.1130/b25627.1.

Sutherland, R., et al. (2007), Do Great Earthquakes Occur on the Alpine Fault in Central South Island, New Zealand?, in *Tectonics at South Island, New Zealand*, edited by D. Okaya, T. Stern and F. Davey, pp. 235-251, AGU Geophysical Monograph Series.

Thomas, A. M., R. M. Nadeau, and R. Burgmann (2009), Tremor-tide correlations and near-lithostatic pore pressure on the deep San Andreas fault, *Nature*, *462*, 1048-1051, doi:10.1038/nature08654.

Toy, V. G., D. Craw, A. F. Cooper, and R. J. Norris (2010), Thermal regime in the central Alpine Fault zone, New Zealand: Constraints from microstructures, biotite chemistry and fluid inclusion data, *Tectonophysics*, *485*, 178-192, doi:10.1016/j.tecto.2009.12.013.

Walcott, R. I. (1978), Present tectonics and late Cenozoic evolution of New Zealand, *Geophysical Journal of the Royal Astronomical Society*, *52*, 137-164, doi:10.1111/j.1365-246X.1978.tb04225.x.

Wallace, L. M., J. Beavan, R. McCaffrey, K. Berryman, and P. Denys (2007), Balancing the plate motion budget in the South Island, New Zealand using GPS, geological and seismological data, *Geophysical Journal International*, *168*, 332-352, doi:10.1111/j.1365-246X.2006.03183.x.

Wech, A. G., and K. C. Creager (2007), Cascadia tremor polarization evidence for plate interface slip, *Geophys. Res. Lett.*, *34*, L22306, doi:10.1029/2007gl031167.

Wech, A. G., and K. C. Creager (2008), Automated detection and location of Cascadia tremor, *Geophys. Res. Lett.*, *35*, L20302, doi:10.1029/2008gl035458.

Wech, A. G., and K. C. Creager (2011), A continuum of stress, strength and slip in the Cascadia subduction zone, *Nature Geoscience*, *4*, 624-628, doi:10.1038/ngeo1215.

Wech, A. G., K. C. Creager, and T. I. Melbourne (2009), Seismic and geodetic constraints on Cascadia slow slip, *J. Geophys. Res.*, *114*, B10316, doi:10.1029/2008jb006090.

Wightman, R., and T. A. Little (2007), Deformation of the Pacific Plate above the Alpine Fault ramp and its relationship to expulsion of metamorphic fluids: An array of backshears, in A Continental Plate Boundary, in *Tectonics at South Island, New Zealand*, edited by D. Okaya, T. Stern and F. Davey, pp. 177-205, AGU Geophysical Monograph Series.